A 3D Printed, Non-Assembly, Passive Dynamic Walking Toy: Design and Analysis

Christian L. Treviño, Joseph D. Galloway II, Pranav A. Bhounsule*

Robotics and Motion Laboratory

Department of Mechanical Engineering,

The University of Texas at San Antonio,

One UTSA Circle, San Antonio, TX 78249, USA.

* Corresponding author email: pranav.bhounsule@utsa.edu

ABSTRACT

In this paper, we present the redesign and analysis of a century old walking toy. Historically, the toy is made up of two wooden pieces including a rear leg and a front leg and body (as a single piece) that are attached to each other by means of a pin joint. When the toy is placed on a ramp and given a slight perturbation, it ambles downhill powered only by gravity. Before the toy can walk successfully it needs careful tuning of its geometry and mass distribution. The traditional technique of manual wood carving offers very limited flexibility to tune the mass distribution and geometry. We have re-engineered the toy to be 3D printed as a single integrated assembly that includes a pin joint and the two legs. After 3D printing, we have to manually break-off the weakly held support material to allow movement of the pin joint. It took us 6 *iterations to progressively tune the leg geometry, mass distribution, and hinge joint tolerances to create our most successful working prototype. The final 3D printed toy needs minimal post-processing and walks reliably on a* 7.87 *degree downhill ramp. Next, we created a computer model of the toy to explain its motion and stability. Parameter studies reveal that the toy exhibits stable walking motion for a fairly wide range of mass distributions. Although 3D printing has been used to create non-assembly articulated kinematic mechanisms, this is the first study that shows that it is possible to create dynamics-based non-assembly mechanisms such as walking toys.*

1 Introduction

Passive dynamic robots are machines that can walk or run downhill using only their natural dynamics. These robots are made by assembling individual parts and by iteratively tuning their dynamics by placing external weights and testing

on a downhill ramp. Each time a new robot is assembled, it needs to go through this iterative tuning. In this paper, we explore the creation of a passive dynamic walking toy using 3D printing. The approach has multiple advantages: (1) the mass distribution can be easily tuned by modifying the CAD dimensions and/or print properties (e.g., in-fill), (2) the joints can be printed within the 3D printed body to create an articulated toy without the need for assembling or for additional tooling, and (3) once a successful design iteration is achieved, multiple toys can be 3D printed with minimal tuning. The disadvantages are the long print times for simple designs and the difficulty in fine control of the mass distribution because of the assumptions made by CAD softwares (e.g., uniform mass distribution). However, it is conceivable that the disadvantages will be overcome with further advances in 3D printing.

2 Background and related work

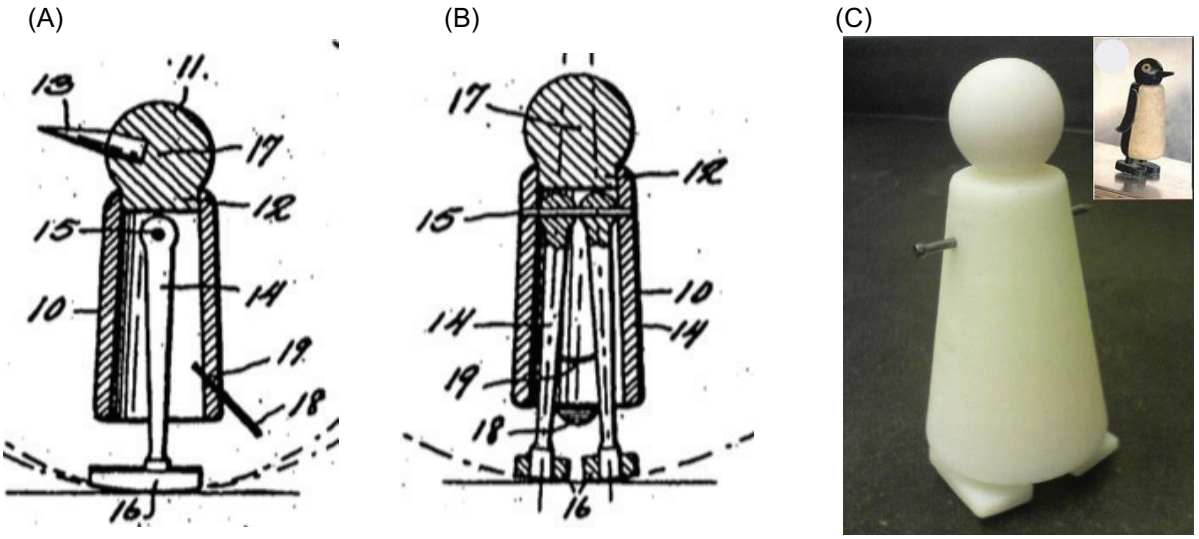

Fig. 1. Wilson Walkie [1] (A) Front view, (B) Side view, (C) A 3D printed wilson walkie and wooden toy in the inset [2]

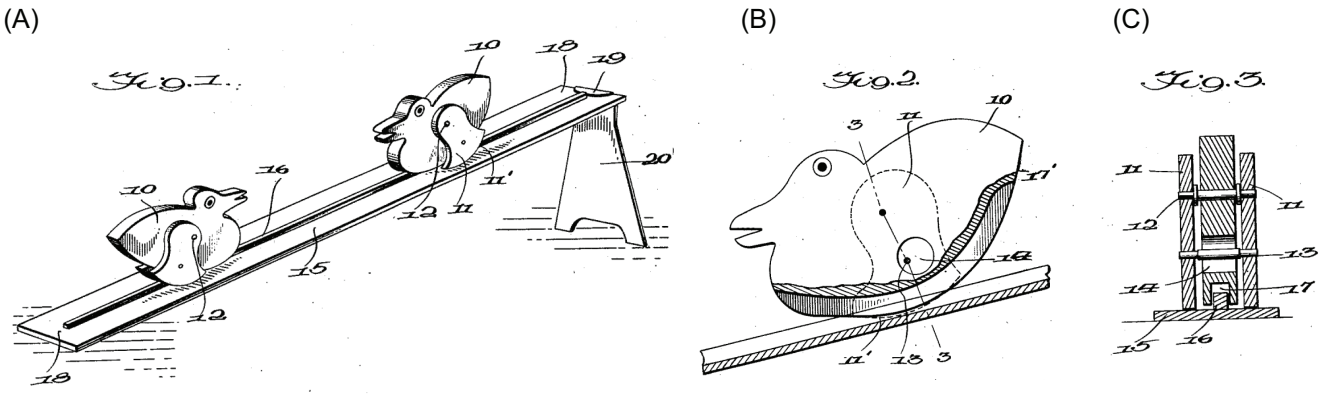

Fig. 2. Ravert Toy (A) Perspective view, (B) Toy duck, (C) Section view of the toy duck (taken from [3])

Passive dynamic toys have been in existence for almost 100 years as evidenced by a number of patents (Fallis 1888 [4], Bechstein 1912 [5], Mahan 1909 [6], Ravert 1932 [3], and Wilson 1938 [1]). We discuss two toy designs.

1. The patent of the Wilson walkie [1] is shown in Fig. 1 (A) and (B). The toy has two legs, each of which connects to a body through a hinge joint. When the toy is launched on a downward incline, the side-ways rocking of the body lifts a foot off the ground. The off-ground foot then swings forward to complete a step. The same sequence is repeated with the other foot and enables the toy to descend downhill.
2. The design of Ravert's toy [3] is shown in Fig. 2. The toy consists of a body (number 10) and two legs (number 11). The body is connected to each leg by a hinge joint (number 12). There is a mechanical stop (number 13) to prevent the legs from overextending. There is a groove in the body (number 17) and the ramp has a guide rib (number 16) that prevents the toy from veering sideways. Both toys are able to descend downhill when given a slight perturbation.

The term "Passive Dynamic Walking" was coined by Tad McGeer [7] who first demonstrated that a human like frame can descend downhill powered only by gravity. While the toy designs mentioned earlier had a rather stiff gait, McGeer's robot had a more human-like appearance. To simplify balance, McGeer constrained his walker to 2D (only front-back or sagittal plane motion) by pairing the inner legs to each other and similarly the outer legs. A true 3D passive dynamic walking robot was built by Collins et. al. [8]. Design features included were curved feet with special guide rails, counter swinging arms, and soft heels to improve stability in side-to-side (coronal plane) and left-right (axial plane) directions. A 2D passive dynamic runner was created by Owaki et al. [9] by adding a torsional spring in the hip and linear springs in the legs. All of these robots are statically stable when their legs are splayed. An interesting idea is to create a legged robot that cannot stand stably but can move stably (like a bicycle). A walking toy based on this concept was created by Coleman [10] and more recently a hopping robot was created by Steinkamp [25].

Gomes and Ahlin [11] created an (almost) passive dynamic walking robot, a rimless wheel, that can move on level ground. Their design involves a hip spring that winds up as the rimless wheel moves from mid-stance to support transfer. The wheel's spoke touches the ground with almost zero speed ensuring a smooth support transfer. On the subsequent step, from support transfer to mid-stance, the spring unwinds to power the rimless wheel. Other successful level ground walking robots exploiting passive dynamic ideas use some or other form of actuation, such as reactive pendulum [12, 13], vibration of beam [14], impulsive ankle push-off [15]. In such cases, actuation is necessary to overcome the energy losses during locomotion (e.g., collisions, internal dissipation due to friction).

Another class of toys are those which rely only on their kinematics to walk, unlike the dynamics-based toys discussed earlier. The simplest kinematic-based toys have a single input (e.g., a crankshaft) which is connected to multiple outputs (e.g., legs) through a series of: gears, levers, and linkages. When the crankshaft is rotated, it sets the gears and/or levers and/or linkages in motion that in turn cause the legs to move, and allow the toy to walk. One example is the Strandbeest, which means "beach beast" when translated, created by Dutch artist Theo Jansen [16]. The original Strandbeest was several feet tall and made up of PVC pipes, but has recently been scaled down and 3D printed. In the Strandbeest, the crankshaft is connected to propellers. The wind causes the propellers to rotate. This rotation is then converted to reciprocating motion

of the legs through a series of linkages, allowing the Strandbeest to walk. More recently, Coros et al. [17] have created a computational framework that allows the non-experts to create animated characters which can then be 3D printed. Lipson et al. [18] provides a history of mechanisms from the Cornell Kinematic Mechanisms collection that can be 3D printed. Since these toys rely only on their kinematics, they are easier to tune in comparison to dynamics based toys discussed in this paper.

There has been limited work done on 3D printing dynamically walking toys. The Wilson Walkie has been 3D printed by Haberland [2] and is shown in Fig. 1 (C). The body and the two legs are printed separately. A nail connects the two legs to the body and also serves as a hinge joint. The toy is able to descend downhill just like the actual wooden Wilson walker shown inset in Fig. 1 (C). More recently, Stöckl [19] has created a toy similar to the Ravert walker [3] and Coleman's tinkertoy [10] but individual pieces were 3D printed and then assembled together. However, it should be possible to change the design to print the entire system monolithically using the same material with a different in-fill for support structure as done in this paper or by using separate support material that dissolves when dipped in appropriate liquid (usually water). The latter is a feature available with newer 3D printers.

Our toy design is loosely based on the Ravert toy walker [3]. In our toy design, the legs are arranged back-to-back instead of sideways (see Fig. 3). The main novelty of this work is the demonstration that dynamic walking toys can be 3D printed as a non-assembly mechanism. More specifically, 3D printing allows us to design and print the toy as a single assembly inclusive of the hinge joint, thus eliminating the manual assembly of the toy. 3D printing has allowed us to tune the mass distribution, while preserving the toy's shape and allowing for quick iteration on the leg geometry. Our final design evolved in just 6 design iterations and was able to walk down a 7.87 degree incline with minimal post processing and is described in Section 3. Further, we created a computer simulation of the model and analyzed the motion and walking stability in Section 4. A discussion of the results is presented in Section 5, followed by conclusion in Section 6.

3 Mechanical Design

Figure 3 shows the final toy design. The toy is based on the mascot of the University of Texas at San Antonio (UTSA) named, "Rowdy" The Roadrunner. The toy has two legs. The front leg is fixed to the body, while the rear leg is attached to the body through a single hinge joint. The hinge joint allows for rotation of the moving leg in the sagittal plane. When the toy is placed on a ramp and perturbed slightly, it walks downhill alternating between the two legs. The toy was 3D printed on Ultimaker 2. A video of the making of the toy and walking motion is in the references [20]. We discuss specific aspects of the toy next. More details are in the Appendix A.

3.1 Hinge design

A hinge joint is used to connect the rear leg to the body and to allow relative motion between the body and the leg. Figure 4 (A) shows a sectional view of the toy and indicates the tolerances on the hinge joint. We designed the hinge joint as follows. We created a circular hole at the top-end of the leg. Next, we aligned the hole with a circular shaft that is designed on the body. The hole was made slightly bigger than the shaft to allow the rear leg to move relative to the shaft on the body. Note that the rear leg is not attached to the body and is floating in free space within the CAD design. While printing the toy,

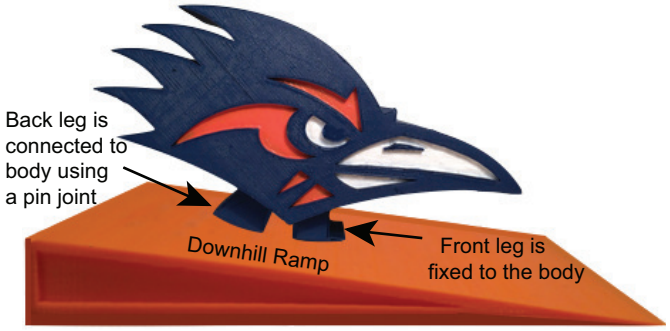

Fig. 3. The final working prototype

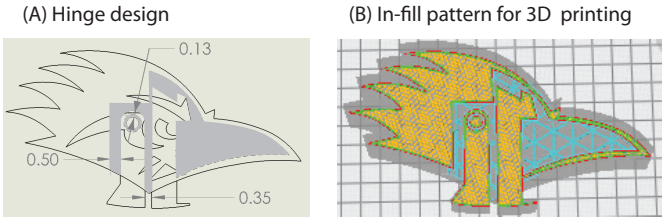

Fig. 4. Sectional view of the design. (A) Hinge design with tolerances. All dimensions are in cm. Shaded areas represents hollow sections. (B) In-fill pattern created by CURA, the post processing software for the 3D printer.

the rear leg is held by support material (PLA with lower material fill than used to print the body). Once the printing was finished, we broke off the support material to allow the rear leg to move.

Our initial prototypes of the printed toy had too little clearance between the circular hole and the shaft so that the rear leg could not move freely. This was because of the limited printing resolution of our desktop 3D printer. We had to manually increase the clearance between the hole and the shaft until we produced a functional hinge joint. The hinge joint has a little bit of play in the transverse and coronal plane, and so the toy tends to veer in one direction during walking sometimes.

3.2 Leg and feet design

There are two legs in our toy design – a front leg that is fixed to the body and a rear leg that is connected to the body using a hinge joint. The rear foot is a circular arc with its center at the hinge joint as shown in Fig. 5. The same radius of curvature is used for the front foot. The shaded area near the rear foot in Fig. 4 (A) show the tolerances around the rear foot. We also found that making the rear (moving) leg to be slightly longer than the front leg leads to a slightly better walking performance than legs of the same length. It is unclear why this asymmetry improves the walking performance.

The toy walks easily on rough surfaces such as wood stock, cardboard, and plywood, yet it slips on aluminum. We created grooves in the transverse direction along the bottom of the feet in attempts of increasing the roughness without successful aid. However, by adding rubber soles to the bottom of the feet, the toy was able to walk on a 3D printed ramp with a slope of 7.87 degrees. The rubber soles were cut from heat shrink tubing and were glued firmly to the base of the feet.

3.3 Tuning the mass distribution

The mass distribution should be such that the center of mass is on the rear leg but beneath the pin joint when the legs are held against each other. We were able to tune the design in CAD so that the mass distribution was between the two legs. However, when the first prototype was printed, the center of mass was found to be in the front resulting in the toy sitting on its beak. The discrepancy was due to the CAD software's estimation of the center of mass based on a uniform mass distribution which is not true when 3D printed.

To tune the mass distribution, we attached known weights to the rear of the toy until it achieved a static standing position. Based on the tuned weight, we then re-adjusted the CAD design by enlarging the feathers and hollowing the beak. The modification was successful in achieving the necessary mass distribution to achieve stable downhill walking.

3.4 Support Material

The role of the support material is to act as a scaffold to brace and hold overhanging and undercut structures while printing, so that the printed plastic does not sag under gravity. In our case, the same PLA that was used for printing the toy was used as support material, except with a lower material fill percentage, allowing for the manual removal once the printing was completed.

In our toy design there are three distinct places where support material is used

1. Support material is placed between the rear leg and the body as shown by the shaded areas in Fig. 4 (A). The support material is manually detached using a screwdriver to allow the rear leg to move.
2. Support material is placed in the hollow section of the beak along the transverse direction to allow 3D printing of the beak as shown in Fig. 4 (B). The support material is inside the toy and cannot be removed once printed.
3. A layer of support material is deposited on the 3D printer bed before the toy is printed. The support material is removed after the printing is completed. We noticed that if the toy is directly printed on the bed, then the face which is placed on the bed gets warped due to the heat of the bed. Thus, the presence of the support material on the bed prevents the side adjoining the bed from warping.

3.5 3D printing

Before 3D printing, the CAD design is pre-processed using CURA, an open source slicing software. At this point we specify 3D printing parameters that include the scaling, the temperature of the nozzle, and the in-fill percentage. We choose an in-fill percentage of 80% for the toy. A higher in-fill percentage increases the print time but too low a value decreases the weight of the toy and this affects its performance. Also, we chose an in-fill percentage of 10% for the hollow section of the beak. Ideally a zero in-fill percentage leads to a perfectly hollow section but a finite value is needed to act as a supporting structure for the upper layers of the printed toy. The chosen value of 10% is the minimal value that allows enough support as the toy is printed. Both the in-fill percentages were decided by trial and error. A visualization of the pattern used by the 3D printing software is shown in Fig. 4 (B). Next the toy is 3D printed on Ultimaker 2, a desktop hobby-grade 3D printer using a 2.85 mm diameter Polyactic Acid (PLA) filament. The print time is about 12 hours, which was 3 hours less than the time

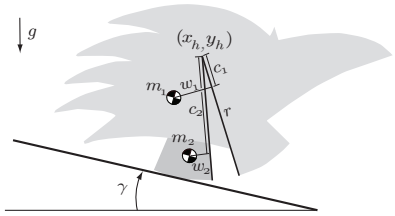

Fig. 5. Robot model for simulation

estimated by CURA. After the printing is complete, we manually remove the supporting material that holds the rear leg in place using a screwdriver.

3.6 Testing

The testing of the toy was initially done on a wooden ramp, but subsequently the toy was able to walk on a 3D printed PLA ramp. First, we set up a ramp inclination. Then, we placed the toy on the ramp and perturbed it slightly by tilting the toy backwards or forwards and releasing it. If the toy was not able to descend downhill, we increased or decreased the inclination a little and tried again. If the toy stopped, then the slope was too small and we needed to increase it. However, if the robot slid downhill or overturned, then the slope was too big and we needed to decrease the slope. For our toy design we have found that a 7.87° or 0.1373 rad incline works best. By adding rubber feet to the soles, the toy is able to descend smooth surfaces such as aluminum.

4 Computer Simulation

4.1 Model

A caricature of the model with the dimensions is shown in Fig. 5. The robot consists of two pieces: (1) The body and front leg as a single unit shown in light gray color (we designate this piece as the front leg), and (2) the rear leg shown in dark gray color. A pin joint connects the two legs together. To derive equations of motion, we use a line of reference fixed on each leg as follows: (1) The reference line for the front leg is along its rear edge with the origin at the pin joint, and (2) the reference line for the rear leg is along its front edge and with the origin at the pin joint. The masses of the front and rear leg are m_1 and m_2 respectively, and the location of the center of mass (COM) measured relative to the line of reference is c_1 and w_1 for the front leg and c_2 and w_2 for the rear leg as shown in the figure. There is a hard stop that limits the angle between the legs (i.e., the angle between the two reference lines on the legs) to α. The leg length is r, gravity is g, and ramp slope is γ. We assume the following kinematics: the leg on the ground is the stance leg with absolute angle q_1 and absolute angular velocity u_1, and the other leg is the swing leg with relative angle q_2 and relative angular velocity u_2.

The equations of motion for a single step are derived using the sequence of phases and transition shown in Fig. 7. Equation 1 represents the sequence of motion for the walker. The equation is a graphical method of representing the motion sequence for a hybrid dynamical system. The phases of motion are defined between the arrows and the transition conditions are defined above the arrows. For example, *One DOF, Front Leg Stance* indicates that the walker moves as a single unit (i.e.,

Fig. 6. A single step of the walker: (Top panel) One step from video. (Bottom panel) Animation from the simulation. See video in the reference for a comparison [21].

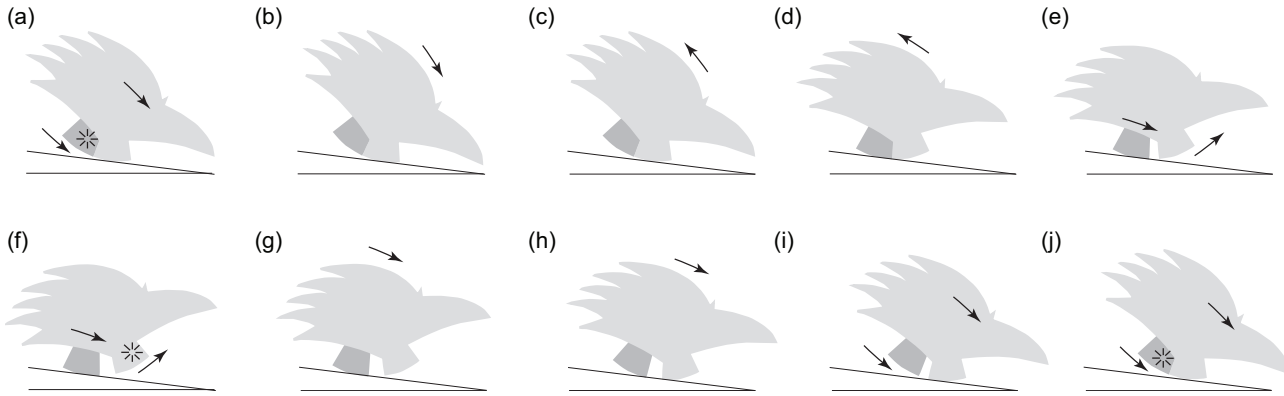

Fig. 7. Sequence of phases and transitions used for simulation model: A single and doubled curved arrow on the figure indicates that the toy is a one or two degree of freedom system in that particular phase.

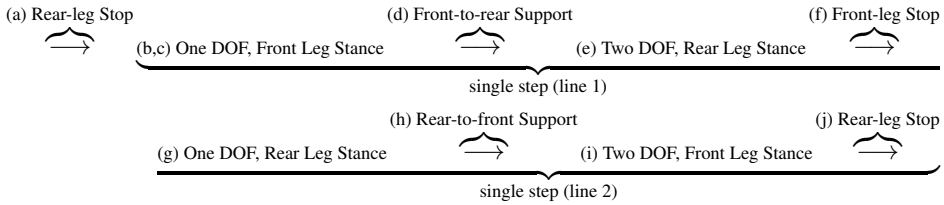

(1)

the swing leg is locked to the stance leg due the angle stop). Then the transition condition, *Front-to-rear Support* occurs wherein the support is transferred from the front leg to the rear leg. This transition leads to phase *Two DOF, Rear Leg Stance*. In this phase, the rear leg is the stance leg and rolls freely and the front leg is the swing leg that pivots about the rear leg – a two degree of freedom system. From Eq. 1 it can be seen that the system is either a 1 DOF or a 2 DOF system during a single step. For the 1 DOF system, we use the angular momentum balance about the contact point of the stance leg to derive an equation for the absolute angular acceleration, $\ddot{q}_1$. For the 2 DOF system, we use the angular momentum balance about the contact point and the pin joint to derive equations for the absolute angular acceleration $\ddot{q}_1$ and $\ddot{q}_2$. The front-to-rear and rear-to-front transitions are smooth and we make an appropriate switch of leg angles (i.e., current stance leg becomes swing leg and vice versa). The front-leg stop and rear-leg stop are non-smooth transitions where the colliding swing leg comes to a stop and the velocity of the stance leg after collision is found by using the conservation of angular momentum about the pin

joint. Please see the supplementary material for additional details (Appendix A).

4.2 Motion analysis: periodic motion and stability

Given an initial state for the system $\mathbf{x} \equiv [q_1, u_1, q_2, u_2]$ and the simulation parameters (see Tab. 1), the equations of motion are integrated forward in time to simulate the motion of the system. We are interested in the periodic motion of the toy. Since the complexities of the equations of motion preclude an analytical solution, we resort to numerical techniques.

Periodic motion is found by treating a walking step as a Poincaré map [7]. Given the state of the system at a particular instant (e.g., front-leg stop, rear-to-front support transfer) of the walking step, $\mathbf{x}_n$, and the state at the same instant but on the next step, $\mathbf{x}_{n+1}$, one can find a function $\mathbf{F}$ that relates the two, $\mathbf{x}_{n+1} = \mathbf{F}(\mathbf{x}_n)$. To find periodic motions, we find a fixed point, $\mathbf{x}^*$ such that, $\mathbf{x}^* = \mathbf{F}(\mathbf{x}^*)$. This is equivalent to finding the zeros of $\mathbf{G}(\mathbf{x}^*) = \mathbf{x}^* - \mathbf{F}(\mathbf{x}^*)$. This is the same as solving 3 equations in 3 unknowns (the Poincaré section reduces the state space from 4 to 3). However, we can reduce the dimension of G from 3 to 1 by choosing the Poincaré section to be at any instant the toy is a single degree of freedom system. For example any of the following stances from Fig. 7 will suffice: (a), (b), (c), (f), or (g) (A similar reduction can be done for the kneed passive dynamic walker, see [22]). We use the instant just after the rear leg comes to a stop after colliding with the front leg (see Fig. 7 (a)). The initial states at this instant are $\mathbf{x_r} \equiv [q_1, u_1]$ and are used in F and G.

The stability of the walking motion is evaluated from the Jacobian of the function $\mathbf{F}$ at the fixed point, i.e., $\mathbf{J}(x_r^*) = \frac{\partial \mathbf{F}(\mathbf{x}_r^*)}{\partial \mathbf{x}_r}$. The system is stable if the largest eigenvalue is less than 1 and unstable otherwise [23]. In our case there are two eigenvalues, but one eigenvalue is zero and corresponds to the perturbation in the direction of the Poincaré section. Thus, the other non-zero eigenvalue gives the stability of the periodic motion.

We used MATLAB to numerically evaluate the functions F and subsequently G. To obtain F, we start the simulation at the instant when the front leg is the stance leg and the rear leg is resting against the front leg (see Eqn. 1 b,c). Subsequently each phase is integrated using *ode113* with a tolerance of 10^{-12}, and the appropriate transition conditions are applied in the order given in Eqn. 1. Thus, given the initial state at the instant the toy moves as a single piece, $\mathbf{x}_r$, F returns the state at the same instant but at the next step. The function G can be numerically obtained once F is found. Next, we use *fsolve* with an accuracy set to 10^{-10} to compute the fixed point. The fixed point of the limit cycle is $\mathbf{x}_r \equiv [-0.0194674275, -1.8975774734]$. Then, we use the central difference of 10^{-5} to evaluate the Jacobian of F and used *eig* to find the two eigenvalues. As expected, one eigenvalue was zero and the other value was 0.436 (< 1) indicating a stable fixed point. The figure 8 shows the phase portrait of the limit cycle.

We compare the fidelity of the model against the toy. We use the open source software Tracker [24] to analyze the motion of the toy. Tracker is able to create time traces of user defined points on the video. We use time traces of the hinge point and points on the two legs to obtain the absolute angles of each leg. Figure 9 shows the comparison between the model and experimental data for a trial run on the ramp. As seen from the plot, the simulation is able to capture the features of the experiment reasonably well. Time snapshots comparing the animations are in Fig. 6 and an accompanying video is in the reference [21].

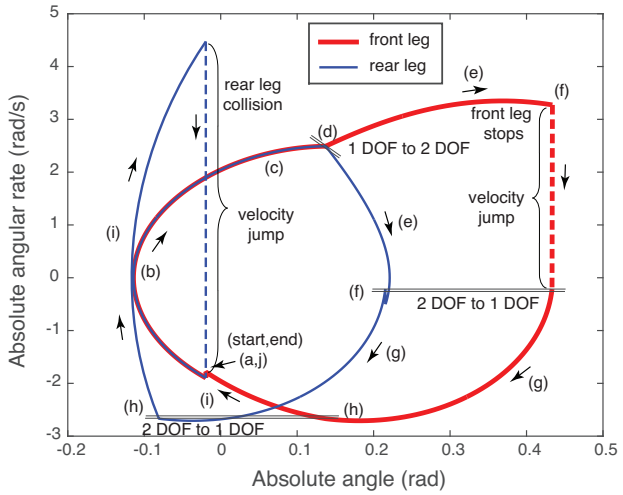

Fig. 8. Phase portrait for the front and rear leg. See corresponding letters in Fig. 7 and Eq. 1.

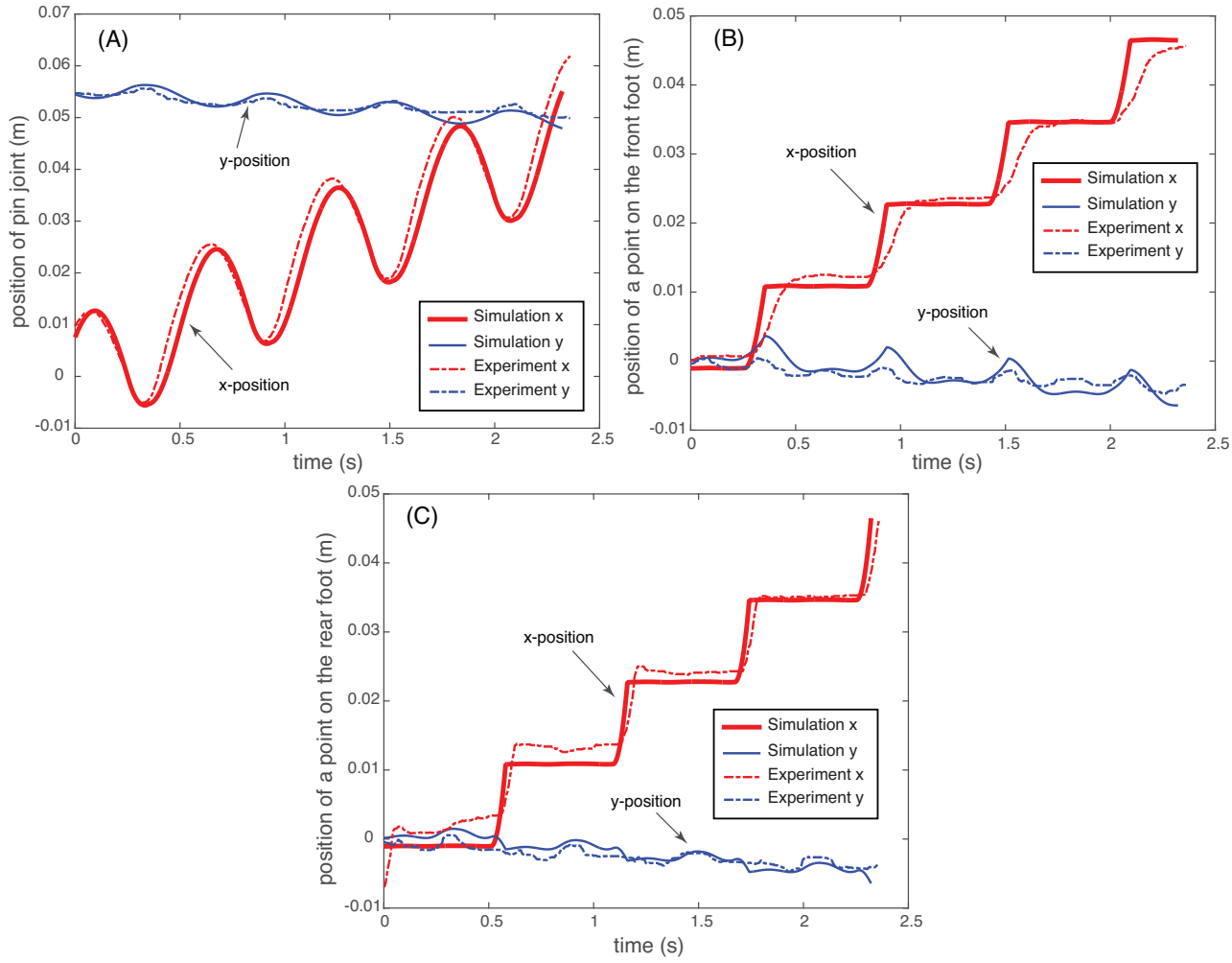

Fig. 9. Comparing simulation with experimental data. Positions of various points on the toy as a function of time. (A) pin joint, (B) bottom corner of the front foot (nearest to the rear foot), (C) bottom corner of the rear foot (nearest to the front foot).

4.3 Parameter study

The Fig. 10 shows the effect of varying three robot parameters, the center of mass of the body (w_1 and c_1) and the leg length (r) on the two limit cycle parameters: the cyclic stability as measured by the maximum eigenvalue and the step velocity, which is non-dimensionalised by dividing by $\sqrt{gr}$. We chose these parameters because they have a substantial effect on the behavior of the toy. The robot parameters were normalized against their nominal values as given in our successful design and presented in Tab. 1. For a given leg radius, we used the simulation technique described in Sec. 4.2 to evaluate the maximum eigenvalue and velocity as a function of center of mass parameters w_1 and c_1. We repeated the calculation for three distinct r values to obtain the plots. Fig. 10 top panel (A), (B), and (C), corresponds to the maximum eigenvalue while bottom panel (D), (E), and (F), corresponds to the velocity. Each pair (A)-(D), (B)-(E), and (C)-(F) corresponds to a distinct r value.

The partial white region in (A), (B), (D), (E) indicates that no limit cycles were found in that region. Note that there are no white regions in (C), (F) indicating that the range of solutions increases as r increases. This trend is consistent: as r is decreased to zero, the region of feasible solutions decreases and there are no limit cycles when $r = 0$. From the top three plots it can be seen that the maximum eigenvalues lie in the range of $0.05 - 0.6$ for a broad range of parameters (note that eigenvalue greater than 1 indicates unstable limit cycle and stability increases as the eigenvalue approaches 0). There is no distinct trend in the eigenvalues and it tends to be discontinuous in some regions. However, we note that the maximum eigenvalues are lowest in (C) on the bottom right corner. This happens when the center of mass along the leg length, c_1, is moved downwards and the fore-aft offset, w_1, is decreased or moved forward relative to our design. The non-dimensional velocity is between 0.02 and 0.035 with maximum velocities occurring at the top right side of each plot. That is, when c_1 moved further down and fore-aft offset w_1 is moved towards the rear. The velocities seem to be smoother and have a more consistent trend than the eigenvalues except in (D) near the white region or where the limit cycles solutions disappear. We found that the limit cycles disappear as w_1 is moved to the edge of the rear leg axis, that is $w_1 \sim 0$. Our design had a maximum eigenvalue of 0.4360 and non-dimensional velocity of 0.0281 and indicated by the black dot in Fig. 10 (B) and (E) respectively.

5 Discussion

We have redesigned an antique walking toy such that it can be 3D printed as a single piece with an integrated hinge joint. After minimal post-processing, the toy is able to walk downhill using its natural dynamics. Then, we created a computer model of the toy, found periodic motion (limit cycles) using Poincaré section, and analyzed motion stability using the eigenvalue of the Jacobian of the limit cycle. We found stable limit cycles for a wide range of parameters. However, all limit cycles had a very slow walking speed, around 0.03 (non-dimensionalised by gravity and leg length).

The use of 3D printing allows us to design and print the complete toy, including the hinge and the rear (moving) leg, as a single assembly. While this eliminates the time needed for assembling the toy, it also makes the design non-modular. Thus, if the hinge joint or the rear leg breaks, then the complete toy needs to be 3D printed again. The use of 3D printing allows us to tune the mass distribution, specifically the location of the center of mass, while preserving the shape of the toy.

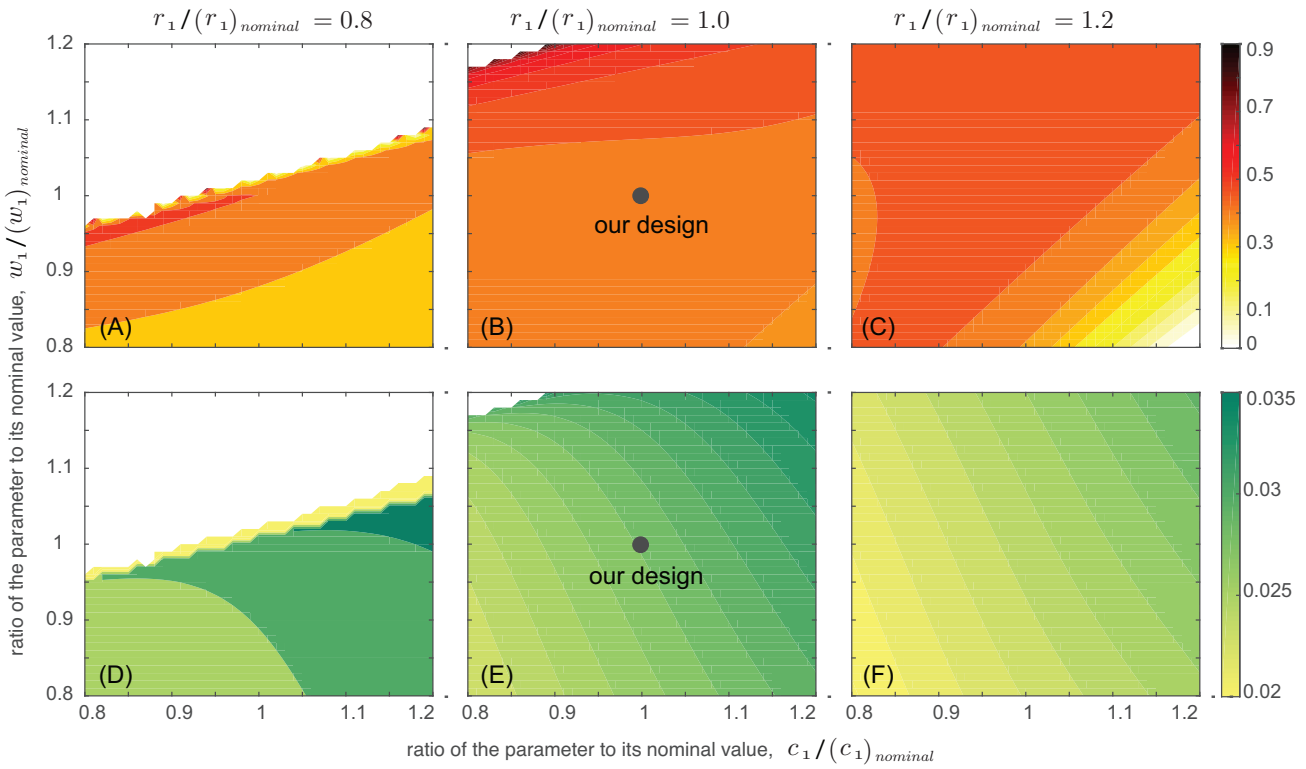

Fig. 10. Effect of varying r, w_1, and c_1 on maximum eigenvalue and velocity. (A,B,C) Maximum Eigenvalue and (D,E,F) Velocity non-dimensionalised by $\sqrt{gr}$. Each parameter r, w_1, and c_1 is non-dimensionalized by its nominal parameter given in Tab. 1. The values for our design is shown using a black dot.

The mass distribution is critical for the toy to walk on the ramp. However, the CAD's estimation of the center of mass is different from the actual center of mass and depends on 3D printing parameters, like scaling and fill percentage. As such, we had to tune the mass distribution by trial and error. The 3D printing pre-processing software CURA does not estimate the center of mass. However, an ability to simulate the 3D printed toy (before actually printing it) would clearly allow for faster tuning. Another issue we faced was that the 3D printer was not able to print the hinge joint to the clearance that we specified in CAD. Ultimately, we had to decrease these tolerances, which lead to play in the hinge joint in both of the transverse and coronal directions. During some of the trials, the play in the transverse direction caused the toy to veer to a particular side.

To enable steady state walking, the total energy loss at each step should balance the potential energy gained. To find the energy loss we proceed as follows. We first compute a periodic solution. Next, we compute the total energy of the system, the sum of kinetic and potential, with respect to the current stance leg at the beginning of each phase of motion described by Eqn. 1. Then by subtracting energy from adjacent phases, we can compute the energy loss in each phase. The sum of all energy losses gives the net gain in potential energy. We found that there are three sources of energy loss: (1) the collision between body and the rear leg (phase (f) Front-leg StopEqn. 1) accounting for 53% of energy loss, (2) the friction between the rear leg and the ground (phase (e) Two dof, rear leg stance Eqn. 1) accounting for 26% of energy loss, and (3) collision of the rear leg with the front leg (phase (j) Rear leg stop Eqn. 1) accounting for the remaining 21%. Since the feet are arcs of a circle with the center at the pin joint, the leg length is equal to the radius of the circle. Thus, the support transfer is smooth and without energy losses. This is the most striking difference between the design and most passive walkers as the latter

have their primary energy loss during support transfer due to collision [7, 8, 10, 25, 26].

The mass distribution is a very important parameter. Since the rear leg is very light compared to the front leg and body, its contribution to the center of mass may be ignored, and a good approximation of the center of mass is that of the front leg and body assembly. The center of mass needs to be below the pin joint but should be located over the rear leg when the toy is placed in a static standing position on level ground with its legs touching each other. If the center of mass is above the front leg or beyond, the toy tends to sit on its beak. If the center of mass is beyond the rear leg, then the toy sits on its feathers. If the center of mass is above the pin joint then the toy is unable to rock back-and-forth (similar to an inverted pendulum) and cannot walk. Our dynamic analysis (see Fig. 10) indicates that following design features are desirable for achieving successful walking motion for a given slope: (1) increase the radius (r) of the leg, (2) move the center of mass away from the hinge joint (c_1) and (3) move the center of mass offset towards the rear of the toy (w_1). Similar observation was made by McGeer on a different model of walking [7].

The largest eigenvalue of the Jacobian of the Poincareé map indicates walking stability. A value less than 1 indicates a stable system and unstable otherwise. Typical passive-dynamic walkers are only mildly stable at best by this measure, with their largest eigenvalues rarely less than about 0.6 in magnitude [27]. However, our analysis indicates that for a range of parameters, the eigenvalues are between 0.05 - 0.6, indicating a highly stable system in comparison to other passive dynamic walkers. However, like other passive dynamic walkers, the toy had a very slow walking speed of about 0.03 (non-dimensionalized by $\sqrt{g\ell}$).

Our work has several limitations which we list next. The location of the center of mass is key to walking performance. However, getting the mass distribution correct required elaborate trial and error. This was because 3D printing does not create homogenous objects and thus the actual center of mass was different from what we designed it to be in the CAD software. The print time for the 157 *gm* toy (dimensions 15cm $\times$ 5cm $\times$ 8 cm) is around 12 hours. This is a significant bottleneck and mass production does not seem feasible. We have searched only for a single period one-limit cycle and one cannot rule out other limit cycles, bifurcations and chaos as observed in other passive walkers [28, 29].

6 Conclusions

We have re-created an antique walking toy using 3D printing. The use of 3D printing allows us to print an integrated design that includes joints and moving parts as a single assembly, and helps tune the mass distribution and leg geometry quickly to realize a working prototype. The toy is able to walk down a 7.87 degree incline using only its mass distribution and geometry. Computer simulation of the model indicates a stable limit cycle with largest eigenvalue of 0.26.

The results from this paper can be used as a starting point in creating dynamically balanced walking robots using 3D printing. Further extensions can include 3D printing joints and actuators as a single integrated piece that will lead to more practical robots [30].

Acknowledgment

This work was partially supported by NSF grant IIS 1566463 to P. Bhounsule. In addition, C. Treviño was supported by a Valero Scholarship from the College of Engineering at UTSA and J. Galloway was supported by the Office of Undergraduate Research scholarship and the McNair Scholars Program at UTSA.

A Multimedia Extension

1. A video of the hardware prototype available on this YouTube link
   `https://youtu.be/wJ3W3MomWl4`.
2. A video comparing the simulation with experiments is on this YouTube link
   `https://youtu.be/sAGWg-DyDOw`.
3. MATLAB code for equation generation and simulation simulation and animation and a text file containing more details on design, printing, and modeling is available on github
   `https://github.com/pab47/RowdyWalker`

References

[1] Wilson, J. E., 1938. Walking toy. US Patent 2140275.

[2] Haberland, M., 2007. Make your own wilson walkie. `http://ruina.tam.cornell.edu/research/history/WilsonWalker/index.php`, Accessed February 2016.

[3] Ravert, W., 1932. Walking toy, May 31. US Patent 1,860,476.

[4] Fallis, G., 1888. Walking toy. U.S. Patent No. 376588.

[5] Bechstein, B., 1912. Improvements in and relating to toys. UK Patent 7453.

[6] Mahan, J. J., and Moran, J. F., 1909. Toy. U.S. Patent No. 1007316.

[7] McGeer, T., 1990. "Passive dynamic walking". *The International Journal of Robotics Research,* **9**(2), p. 62.

[8] Collins, S., Wisse, M., and Ruina, A., 2001. "A three-dimensional passive-dynamic walking robot with two legs and knees". *The International Journal of Robotics Research,* **20**(7), p. 607.

[9] Owaki, D., Koyama, M., Yamaguchi, S., Kubo, S., and Ishiguro, A., 2011. "A 2-d passive-dynamic-running biped with elastic elements". *Robotics, IEEE Transactions on,* **27**(1), pp. 156–162.

[10] Coleman, M., and Ruina, A., 1998. "An uncontrolled walking toy that cannot stand still". *Physical Review Letters,* **80**(16), pp. 3658–3661.

[11] Gomes, M. W., and Ahlin, K., 2015. "Quiet (nearly collisionless) robotic walking". In Robotics and Automation (ICRA), 2015 IEEE International Conference on, pp. 5761–5766.

[12] Iida, F., Dravid, R., and Paul, C., 2002. "Design and control of a pendulum driven hopping robot". In Intelligent Robots and Systems, 2002. IEEE/RSJ International Conference on, Vol. 3, IEEE, pp. 2141–2146.

[13] Zoghzoghy, J., and Hurmuzlu, Y., 2014. "Pony ii robot: inertially actuated baton with double-action pendu-

lums". In ASME 2014 Dynamic Systems and Control Conference, American Society of Mechanical Engineers, pp. V001T11A002–V001T11A002.

[14] Reis, M., and Iida, F., 2014. "An energy-efficient hopping robot based on free vibration of a curved beam". *IEEE/ASME Transactions on Mechatronics,* **19**(1), pp. 300–311.

[15] Collins, S. H., and Ruina, A., 2005. "A bipedal walking robot with efficient and human-like gait". In Proceedings of the 2005 IEEE International Conference on Robotics and Automation, pp. 1983–1988.

[16] Jansen, T., 2016. Strandbeest. `http://www.strandbeest.com/`, Accessed February 2016.

[17] Coros, S., Thomaszewski, B., Noris, G., Sueda, S., Forberg, M., Sumner, R. W., Matusik, W., and Bickel, B., 2013. "Computational design of mechanical characters". *ACM Transactions on Graphics (TOG),* **32**(4), p. 83.

[18] Lipson, H., Moon, F. C., Hai, J., and Paventi, C., 2005. "3-d printing the history of mechanisms". *Journal of Mechanical Design,* **127**(5), pp. 1029–1033.

[19] Stöckli, F., Modica, F., and Shea, K., 2016. "Designing passive dynamic walking robots for additive manufacture". *Rapid Prototyping Journal,* **22**(5), pp. 842–847.

[20] Trevino, C. L., 2017. Rowdy-walker, a downhill walking toy. `https://youtu.be/wJ3W3MomWl4`, Accessed July 2017.

[21] Galloway, J., 2017. Rowdy walker: comparing model with simulation. `https://youtu.be/sAGWg-DyDOw`, Accessed July 2017.

[22] McGeer, T., 1990. "Passive walking with knees". In Robotics and Automation, 1990. Proceedings., 1990 IEEE International Conference on, IEEE, pp. 1640–1645.

[23] Strogatz, S. H., 2006. *Nonlinear dynamics and chaos: with applications to physics, biology, chemistry and engineering*. Perseus Publishing.

[24] Brown, D., 2016. Tracker, video analysis and modeling tool. World Wide Web electronic publication.

[25] Steinkamp, P., 2017. "A statically unstable passive hopper: Design evolution". *Journal of Mechanisms and Robotics,* **9**(1), p. 011016.

[26] Stiesberg, G., van Oijen, T., and Ruina, A., 2017. "Steinkamp's toy can hop 100 times but can't stand up". *Journal of Mechanisms and Robotics,* **9**(1), p. 011017.

[27] Bhounsule, P. A., Cortell, J., Grewal, A., Hendriksen, B., Karssen, J. D., Paul, C., and Ruina, A., 2014. "Low-bandwidth reflex-based control for lower power walking: 65 km on a single battery charge". *The International Journal of Robotics Research,* **33**(10), pp. 1305–1321.

[28] Garcia, M., Chatterjee, A., Ruina, A., and Coleman, M., 1998. "The simplest walking model: stability, complexity, and scaling". *Journal of biomechanical engineering,* **120**(2), pp. 281–288.

[29] Thuilot, B., Goswami, A., and Espiau, B., 1997. "Bifurcation and chaos in a simple passive bipedal gait". In Robotics and Automation, 1997. Proceedings., 1997 IEEE International Conference on, Vol. 1, IEEE, pp. 792–798.

[30] MacCurdy, R., Katzschmann, R., Kim, Y., and Rus, D., 2016. "Printable hydraulics: a method for fabricating robots by 3d co-printing solids and liquids". In Robotics and Automation (ICRA), 2016 IEEE International Conference on,

IEEE, pp. 3878–3885.

List of Tables

1 Simulation parameters 12

List of Figures

1 Wilson Walkie [1] (A) Front view, (B) Side view, (C) A 3D printed wilson walkie and wooden toy in the inset [2] 2

2 Ravert Toy (A) Perspective view, (B) Toy duck, (C) Section view of the toy duck (taken from [3]) 2

3 The final working prototype 3

4 Sectional view of the design. (A) Hinge design with tolerances. All dimensions are in cm. Shaded areas represents hollow sections. (B) In-fill pattern created by CURA, the post processing software for the 3D printer. 3

5 Robot model for simulation 5

6 A single step of the walker: (Top panel) One step from video. (Bottom panel) Animation from the simulation. See video in the reference for a comparison [21]. 6

7 Sequence of phases and transitions used for simulation model: A single and doubled curved arrow on the figure indicates that the toy is a one or two degree of freedom system in that particular phase. 6

8 Phase portrait for the front and rear leg. See corresponding letters in Fig. 7 and Eq. 1. 7

9 Comparing simulation with experimental data. Positions of various points on the toy as a function of time. (A) pin joint, (B) bottom corner of the front foot (nearest to the rear foot), (C) bottom corner of the rear foot (nearest to the front foot). 7

10 Effect of varying r, w_1, and c_1 on maximum eigenvalue and velocity. (A,B,C) Maximum Eigenvalue and (D,E,F) Velocity non-dimensionalised by $\sqrt{gr}$. Each parameter r, w_1, and c_1 is non-dimensionalized by its nominal parameter given in Tab. 1. The values for our design is shown using a black dot. 8

Table 1. Simulation parameters

Symbol	Value	Description
m_1	141 gm	Mass of body
m_2	16 gm	Mass of rear leg
I_1	1300 $gm\text{-}cm^2$	Inertia of body about center of mass
I_2	30 $gm\text{-}cm^2$	Inertia of rear leg about center of mass
r	5.5 cm	Leg length
c_1	1.93 cm	Distance of front leg COM along leg axis
w_1	0.00075 cm	Distance of front leg COM normal to leg axis
c_2	3.85 cm	Distance of rear leg COM along leg axis
w_2	0.00071 cm	Distance of rear COM normal to leg axis
g	9.81 m/s^2	Gravitational constant
γ	0.1372 rad	Ramp slope
α	0.2182 rad	Maximum angle between the legs
C_1	0.005 Ns/n	Viscous friction betn. rear leg & ground

MULTIMEDIA EXTENSION

ASME Journal of Mechanisms and Robotics

Supplementary Information

for the paper

A 3D Printed, Non-Assembly, Passive Dynamic Walking Toy: Design and Analysis

Most recent modification on March 14, 2018.

Christian L. Treviño, Joseph Galloway, Pranav A. Bhounsule*,
Robotics and Motion Laboratory
Dept. of Mechanical Engineering,
University of Texas San Antonio
One UTSA Circle, San Antonio, TX 78249, USA.
* Corresponding author email: pranav.bhounsule@utsa.edu

1 Notation

1.1 Robot parameters

Symbol	Value	Parameter description
m_1	141 gm	Mass of body.
m_2	16 gm	Mass of rear leg.
I_1	1300 $gm - cm^2$	Inertia of body.
I_2	30 $gm - cm^2$	Inertia of rear leg.
r	5.5 cm	Leg length.
c_1	1.76 cm	Distance of body COM along leg axis (positive is downward).
w_1	0.75×10^{-3} cm	Distance of body COM normal to leg axis (positive is backward).
c_2	3.85 cm	Distance of rear leg COM along leg axis (positive is downward).
w_2	0.71×10^{-3} cm	Distance of rear leg COM normal to leg axis (positive is backward).
g	9.81 m/s^2	Gravitational constant.
γ	0.1372 rad	Ramp slope.
α	0.2182 rad	Maximum angle between the legs.
C_1	0.005 Ns/m	Viscous friction between rear leg and ground.

1.2 Simulation variables

Symbol	Variable description
t	time.
q_1	absolute angle between the stance leg and normal to the ramp.
q_2	relative angle between the swing leg and the stance leg.

u_1	angular velocity of the stance leg ($= \dot{q}_1$).
u_2	angular velocity of the swing leg ($= \dot{q}_2$).
q_1^+, q_1^-	absolute angle of the stance leg wrt. vertical after and before transition.
u_1^+, u_1^-	angular velocity of the stance leg wrt. vertical after and before transition.
q_2^+, q_2^-	relative angle of the swing leg wrt. stance leg after and before transition.
u_2^+, u_2^-	angular velocity of the swing leg wrt. stance leg after and before transition.
$\vec{H}^+_{/P}$ $\vec{H}^-_{/P}$	Angular momentum about point P after and before transition.
$\dot{\vec{H}}_{/P}$	Rate of change of angular momentum about point P and so on.
$\vec{M}_{/P}$	External angular moment about point P and so on.

2 Toy Design and 3D printing

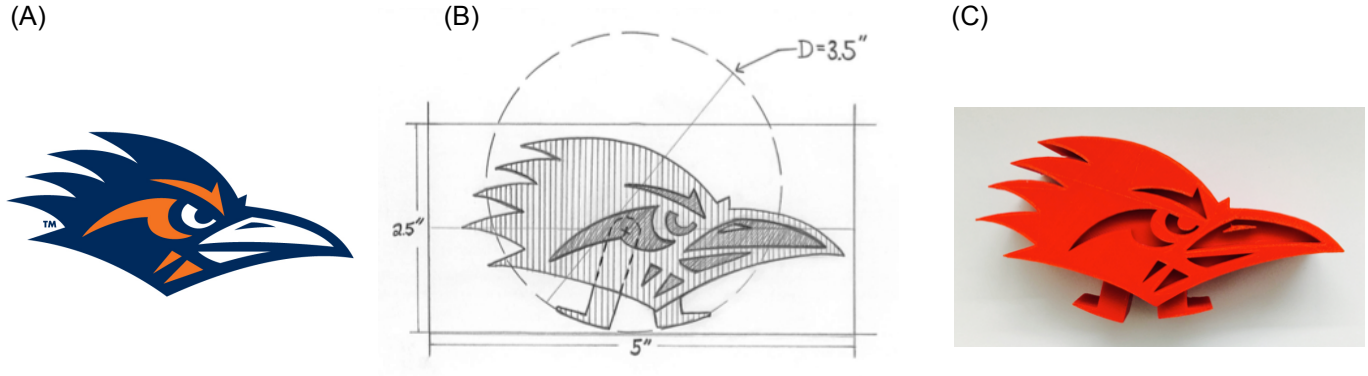

Figure 1: (A) UTSA Mascot "Rowdy" The Roadrunner Logo [2], (B) a sketch of the toy, and (C) a CAD rendering of the toy

The Fig. 1 (A) shows the UTSA mascot from the University's Communications and Marketing website. The goal of the design stage was to add legs to the mascot, followed by tuning the mass distribution, leg geometry, and the tolerances on the hinge joint to create a functional walking prototype. The Fig. 1 (B) shows the initial sketch of the toy with legs and Fig. 1 (C) shows a 3D CAD rendering of the sketch that was drawn using SOLIDWORKS.

Next, the toy was pre-processed using CURA, an open source slicing software. CURA divides the CAD drawing into a number of slices as shown in Fig. 2. We also needed to specify other 3D printing options at this stage. The specifications included the: scaling, temperature of the nozzle, material fill for the toy and/or the support material. Note that we can only choose the in-fill for one of the two, toy or the support material and the other in-fill is automatically determined by CURA. These specifications are given in Tab. 1. CURA estimated the print time to be 15 hours.

Next the toy was printed using an Ultimaker 2, a desktop hobby-grade 3D printer. We used a 2.85mm diameter Polyactic Acid (PLA) filament for 3D printing. The print time was about 12 hours, which was less than the time estimated by CURA. After the printing was completed, we removed the toy from the heated print bed. Next, we removed any supporting material on the

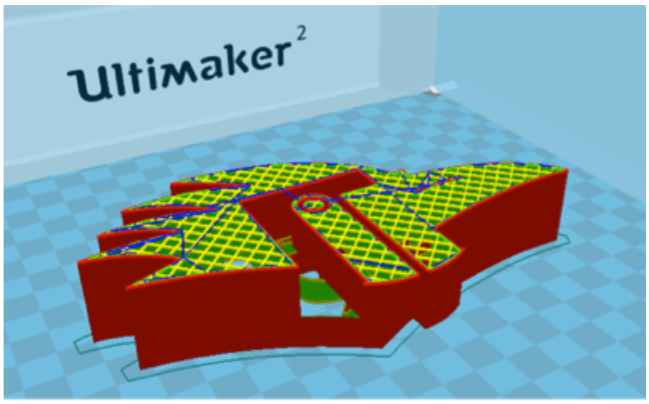

Figure 2: The CAD Drawing Is Pre-processed Before It Is 3D Printed Using Cura, A Slicing Software

Table 1: 3D Printing Parameters

Parameter	Value
Fill density for toy	80 %
Fill density for support material	10%.
Scaling (CAD:3D-printing)	3:4
Nozzle temperature	220 °C

body that surrounded the moving leg, using a combination of a screwdriver and manual shaking. The toy is able to walk downhill on a 7.87 degree when given a slight perturbation.

Additionally, we have explored painting the toy to correspond to the UTSA brand identity colors. The final colored toy is shown in Fig. 3. The main reason for painting the toy was the unavailability of a PLA spool corresponding to UTSA brand identity colors. Acrylic paint is normally used to paint PLA plastic. We used acrylic to paint the white portion of the toy. Due to the non-availability of UTSA brand blue and orange colors in acrylic, we used Valspar signature semi-gloss interior high-hiding paint and primer. First, we cleaned the toy of all the support material using needle nose pliers and needle files. Then, we sanded by hand all of the sharp edges with a fine grit sand paper. We removed the sanding dust from the crevices of the plastic using a toothbrush dipped in dish soap. The toy was washed and then left to dry. Once fully dry, we painted the toy by applying 5 layers of Valspar's paint due to the strong initial absorption of the PLA. We allowed the paint to dry out before painting successive layers to avoid clumping of the paint. The sanding and hand painting took about 10 hours. However, by using a sheet sander and an airbrush, we were able to reduce the time to less than 2 hours. Finally, the toy was sealed with 2 coats of Valspar premium finish paint and primer Micromist finishing spray.

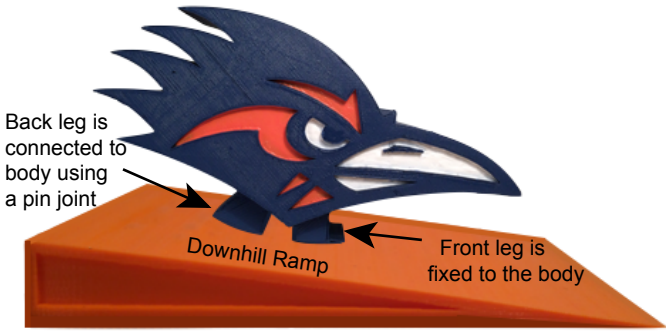

Figure 3: The Final Product

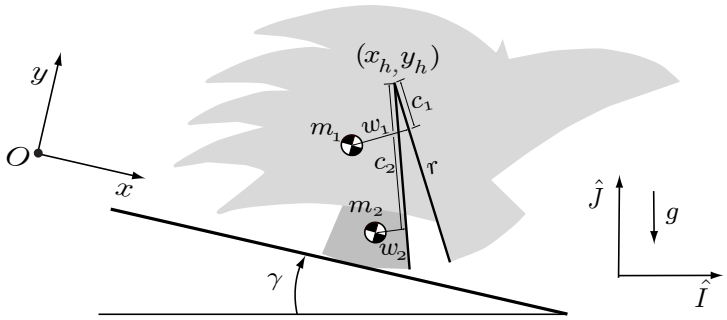

Figure 4: **The model:** The robot consists of two pieces: (1) The body and front leg (light gray) is a single unit (we designate this piece as the body + front-leg), and (2) the rear leg (dark gray). The rear leg connects to body + front-leg by means of a pin joint.

3 Modelling Details

A caricature of the model with the dimensions and frames of reference is shown in Fig. 4. A single step of the walker is shown in Fig. 5 and is referenced in the equation below

$$\underbrace{\overset{\text{(a) Rear-leg Stop}}{\overbrace{\longrightarrow}}\ \overset{\text{(b,c) One DOF, Front Leg Stance}}{\overbrace{\longrightarrow}}\ \overset{\text{(d) Front-to-rear Support}}{\overbrace{\longrightarrow}}\ \overset{\text{(e) Two DOF, Rear Leg Stance}}{\overbrace{\longrightarrow}}\ \overset{\text{(f) Front-leg Stop}}{\overbrace{\longrightarrow}}}_{\text{single step (line 1)}}$$
$$\underbrace{\overset{\text{(g) One DOF, Rear Leg Stance}}{\overbrace{\longrightarrow}}\ \overset{\text{(h) Rear-to-front Support}}{\overbrace{\longrightarrow}}\ \overset{\text{(i) Two DOF, Front Leg Stance}}{\overbrace{\longrightarrow}}\ \overset{\text{(j) Rear-leg Stop}}{\overbrace{\longrightarrow}}}_{\text{single step (line 2)}} \tag{1}$$

Transition conditions are above the arrow and phases of motion are between the arrows. For example, *One DOF, Front Leg Stance* indicates that the walker moves as a single unit (i.e., the swing leg is locked to the stance leg due the angle stop). Then the transition condition, *Front-to-rear Support* occurs wherein the support is transferred from the body+front-leg to the rear-leg.

This transition leads to phase *Two DOF, Rear Leg Stance*. In this phase, the rear-leg is the stance leg and rolls freely and the body+front-leg is the swing leg that pivots about the rear-leg – a two degree of freedom system.

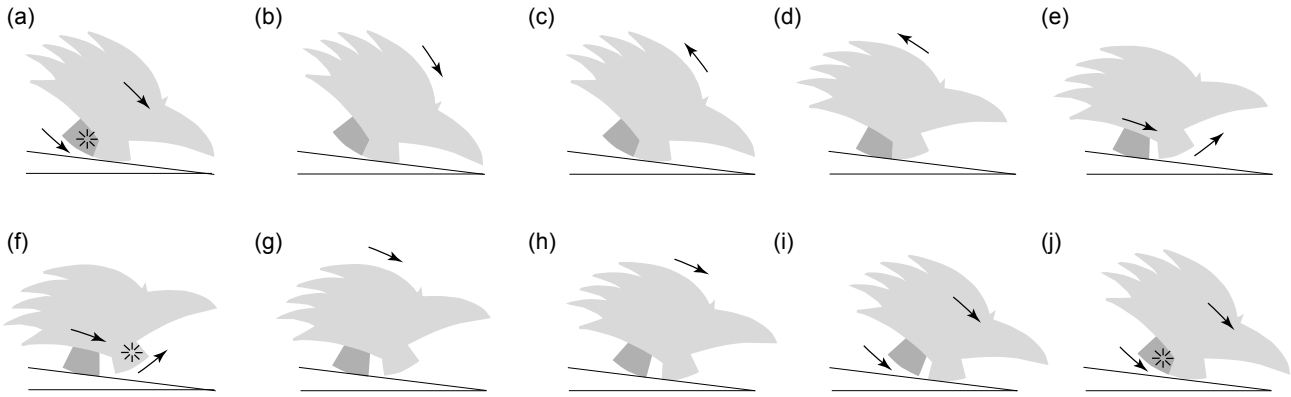

Figure 5: **A single step of the walker:** See Eq.(1) for more details.

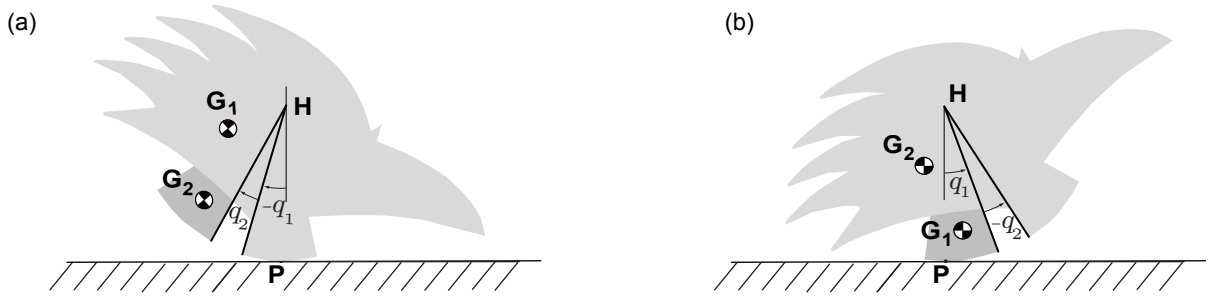

Figure 6: **Angles and naming convention for deriving the equations for the two modes:** (a) Front leg is the stance leg. (b) Rear leg is the stance leg. P is the contact point with the ground.

Equations of motion

Next, we describe the derivation of the equations for each phase and transition. We reference the transitions/phases in the order shown in Eq. (1) and Fig. 5. The equations were derived using the *Symbolic Toolbox* in MATLAB. All MATLAB files are provided on github [1].

3.1 One DOF, Front Leg Stance (see Fig. 5 (b,c))

In this phase, the body+front-leg is the stance leg (see Fig. 6 (a)) and the rear-leg rests against the stance leg. Thus, the dynamics of the system are due to q_1, whereas $q_2 = u_2 = 0$. The equations

are

$$A\ddot{q}_1 = b,$$
$$\ddot{q}_2 = 0.$$

The first equation used angular momentum balance about the contact point $\dot{\vec{H}}_{/P} = \vec{M}_{/P}$ and second equation is because the swing leg is stationary relative to the stance leg. The A and b matrices are

$$\begin{aligned} A = {} & 2\,\mathrm{c_1}\,\mathrm{m_1}\,r\,\cos(\mathrm{q_1}) - {\mathrm{c_2}}^2\,\mathrm{m_2} - \mathrm{m_1}\,r^2 - \mathrm{m_2}\,r^2 - \mathrm{m_1}\,{\mathrm{w_1}}^2 - \mathrm{m_2}\,{\mathrm{w_2}}^2 - {\mathrm{c_1}}^2\,\mathrm{m_1} \\ & + 2\,\mathrm{m_1}\,r\,\mathrm{w_1}\,\sin(\mathrm{q_1}) + 2\,\mathrm{c_2}\,\mathrm{m_2}\,r\,\cos(\mathrm{q_1} - \mathrm{q_2}) + 2\,\mathrm{m_2}\,r\,\mathrm{w_2}\,\sin(\mathrm{q_1} - \mathrm{q_2}) - I_1 - I_2 \end{aligned}$$

$$\begin{aligned} b = {} & g\,\mathrm{m_1}\,r\,\sin(\gamma) - g\,\mathrm{m_2}\,\mathrm{w_2}\,\cos(\gamma - \mathrm{q_1} + \mathrm{q_2}) - \mathrm{c_2}\,g\,\mathrm{m_2}\,\sin(\gamma - \mathrm{q_1} + \mathrm{q_2}) \\ & + g\,\mathrm{m_2}\,r\,\sin(\gamma) - \mathrm{c_1}\,g\,\mathrm{m_1}\,\sin(\gamma - \mathrm{q_1}) - g\,\mathrm{m_1}\,\mathrm{w_1}\,\cos(\gamma - \mathrm{q_1}) + \mathrm{c_1}\,\mathrm{m_1}\,r\,{\mathrm{u_1}}^2\,\sin(\mathrm{q_1}) \\ & - \mathrm{m_1}\,r\,{\mathrm{u_1}}^2\,\mathrm{w_1}\,\cos(\mathrm{q_1}) + \mathrm{c_2}\,\mathrm{m_2}\,r\,{\mathrm{u_1}}^2\,\sin(\mathrm{q_1} - \mathrm{q_2}) - \mathrm{m_2}\,r\,{\mathrm{u_1}}^2\,\mathrm{w_2}\,\cos(\mathrm{q_1} - \mathrm{q_2}) \end{aligned}$$

The total energy at the beginning of this phase is found using the formula and using appropriate values for the state.

$$\begin{aligned} E = {} & \frac{\mathrm{I_1}\,{\mathrm{u_1}}^2}{2} + \frac{\mathrm{I_2}\,{\mathrm{u_1}}^2}{2} \\ & + \frac{\mathrm{m_2}\left({\mathrm{u_1}}^2\,(\mathrm{c_2}\,\sin(\mathrm{q_1} - \mathrm{q_2}) - \mathrm{w_2}\,\cos(\mathrm{q_1} - \mathrm{q_2}))^2 + (r\,\mathrm{u_1} - \mathrm{u_1}\,(\mathrm{c_2}\,\cos(\mathrm{q_1} - \mathrm{q_2}) + \mathrm{w_2}\,\sin(\mathrm{q_1} - \mathrm{q_2})))^2\right)}{2} \\ & + \frac{\mathrm{m_1}\left({\mathrm{u_1}}^2\,(\mathrm{c_1}\,\sin(\mathrm{q_1}) - \mathrm{w_1}\,\cos(\mathrm{q_1}))^2 + (r\,\mathrm{u_1} - \mathrm{u_1}\,(\mathrm{c_1}\,\cos(\mathrm{q_1}) + \mathrm{w_1}\,\sin(\mathrm{q_1})))^2\right)}{2} \\ & - g\,\mathrm{m_2}\,(\cos(\gamma)\,(\mathrm{c_2}\,\cos(\mathrm{q_1} - \mathrm{q_2}) - r + \mathrm{w_2}\,\sin(\mathrm{q_1} - \mathrm{q_2})) \\ & \qquad - \sin(\gamma)\,(\mathrm{q_1}\,r - \mathrm{c_2}\,\sin(\mathrm{q_1} - \mathrm{q_2}) + \mathrm{w_2}\,\cos(\mathrm{q_1} - \mathrm{q_2}))) \\ & + g\,\mathrm{m_1}\,(\sin(\gamma)\,(\mathrm{q_1}\,r - \mathrm{c_1}\,\sin(\mathrm{q_1}) + \mathrm{w_1}\,\cos(\mathrm{q_1})) - \cos(\gamma)\,(\mathrm{c_1}\,\cos(\mathrm{q_1}) - r + \mathrm{w_1}\,\sin(\mathrm{q_1}))) \end{aligned}$$

3.2 Front-to-rear Support Transition (see Fig. 5 (d))

The support transfer from body+front-leg to rear-leg occurs when the line joining the pin joint to the rear edge of the front leg is vertical, that is, along direction of gravity. Mathematically, the transition condition is $q_1 = \gamma$. The transition is smooth (i.e., there is no instantaneous change in angular velocity) because both legs have the same length and curvature. Because q_1 and q_2 denotes the position of the stance leg and swing leg respectively, we need to swap the roles of the legs. The conditions are

$$q_1^+ = q_1^- - q_2^-, \qquad u_1^+ = u_1^- - u_2^-, \tag{2}$$
$$q_2^+ = -q_2^- = 0, \qquad u_2^+ = -u_2^- = 0. \tag{3}$$

3.3 Two DOF, Rear Leg Stance (see Fig. 5 (e))

In this phase, the rear-leg is the stance leg and the body+front-leg is the swing leg. We obtain two equations by use angular momentum balance about the contact point, $\dot{\vec{H}}_{/P} = \vec{M}_{/P}$, and about the

pin joint, $\dot{\vec{H}}_{/H} = \vec{M}_{/HP}$ (see Fig. 6 (b)). The equations are of the form

$$\mathbf{A}\ddot{\mathbf{q}} = \mathbf{b},$$

where $\mathbf{q} = \{q_1,\ q_2\}$, $\mathbf{A}$ is a 2x2 matrix, and $\mathbf{b}$ is a 2x1 vector. If $A_{i,j}$ is the element on the ith row and jth of $\mathbf{A}$, and if b_i is the ith row of $\mathbf{b}$ then

$$\begin{aligned} A_{1,1} = &-I_1 - I_2 - 2\,\mathrm{c_2}\,\mathrm{m_2}\,r\,\cos(\mathrm{q_1}) - {\mathrm{c_2}}^2\,\mathrm{m_2} - \mathrm{m_1}\,r^2 - \mathrm{m_2}\,r^2 - \mathrm{m_1}\,{\mathrm{w_1}}^2 - \mathrm{m_2}\,{\mathrm{w_2}}^2 \\ &- {\mathrm{c_1}}^2\,\mathrm{m_1} + 2\,\mathrm{m_2}\,r\,\mathrm{w_2}\,\sin(\mathrm{q_1}) + 2\,\mathrm{c_1}\,\mathrm{m_1}\,r\,\cos(\mathrm{q_1} - \mathrm{q_2}) + 2\,\mathrm{m_1}\,r\,\mathrm{w_1}\,\sin(\mathrm{q_1} - \mathrm{q_2}), \end{aligned}$$

$$\begin{aligned} A_{1,2} &= A_{2,1}, \\ &= I_1 + \mathrm{m_1}\,\left({\mathrm{c_1}}^2 - 1\,r\,\cos(\mathrm{q_1} - \mathrm{q_2})\,\mathrm{c_1} + {\mathrm{w_1}}^2 - 1\,r\,\sin(\mathrm{q_1} - \mathrm{q_2})\,\mathrm{w_1}\right), \end{aligned}$$

$$A_{2,2} = \mathrm{m_1}\,\left({\mathrm{c_1}}^2 + {\mathrm{w_1}}^2\right) + \mathrm{I_1},$$

$$\begin{aligned} b_1 = &\,\mathrm{c_1}\,\mathrm{u_1} - \mathrm{c_1}\,g\,\mathrm{m_1}\,\sin(\gamma - \mathrm{q_1} + \mathrm{q_2}) - g\,\mathrm{m_1}\,\mathrm{w_1}\,\cos(\gamma - \mathrm{q_1} + \mathrm{q_2}) + g\,\mathrm{m_1}\,r\,\sin(\gamma) + g\,\mathrm{m_2}\,r\,\sin(\gamma) \\ &- \mathrm{c_2}\,g\,\mathrm{m_2}\,\sin(\gamma - \mathrm{q_1}) - g\,\mathrm{m_2}\,\mathrm{w_2}\,\cos(\gamma - \mathrm{q_1}) + \mathrm{c_2}\,\mathrm{m_2}\,r\,{\mathrm{u_1}}^2\,\sin(\mathrm{q_1}) - \mathrm{m_2}\,r\,{\mathrm{u_1}}^2\,\mathrm{w_2}\,\cos(\mathrm{q_1}) \\ &+ \mathrm{c_1}\,\mathrm{m_1}\,r\,{\mathrm{u_1}}^2\,\sin(\mathrm{q_1} - \mathrm{q_2}) + \mathrm{c_1}\,\mathrm{m_1}\,r\,{\mathrm{u_2}}^2\,\sin(\mathrm{q_1} - \mathrm{q_2}) - \mathrm{m_1}\,r\,{\mathrm{u_1}}^2\,\mathrm{w_1}\,\cos(\mathrm{q_1} - \mathrm{q_2}) \\ &- \mathrm{m_1}\,r\,{\mathrm{u_2}}^2\,\mathrm{w_1}\,\cos(\mathrm{q_1} - \mathrm{q_2}) - 2\,\mathrm{c_1}\,\mathrm{m_1}\,r\,\mathrm{u_1}\,\mathrm{u_2}\,\sin(\mathrm{q_1} - \mathrm{q_2}) + 2\,\mathrm{m_1}\,r\,\mathrm{u_1}\,\mathrm{u_2}\,\mathrm{w_1}\,\cos(\mathrm{q_1} - \mathrm{q_2}), \end{aligned}$$

$$b_2 = g\,\mathrm{m_1}\,\left(\cos(\gamma)\,\left(\mathrm{c_1}\,\sin(\mathrm{q_1} - \mathrm{q_2}) - \mathrm{w_1}\,\cos(\mathrm{q_1} - \mathrm{q_2})\right) - \sin(\gamma)\,\left(\mathrm{c_1}\,\cos(\mathrm{q_1} - \mathrm{q_2}) + \mathrm{w_1}\,\sin(\mathrm{q_1} - \mathrm{q_2})\right)\right).$$

We have added a viscous damping term, $C_1 \times u_1$ to b_1, to dampen unstable rocking motion of the rear leg. The total energy at the beginning of this phase is found using the formula and using appropriate values for the state.

$$\begin{aligned} E = &\frac{\mathrm{m_1}\,\left(\left(\left(\mathrm{c_1}\,\cos(\mathrm{q_1} - \mathrm{q_2}) + \mathrm{w_1}\,\sin(\mathrm{q_1} - \mathrm{q_2})\right)\,\left(\mathrm{u_1} - \mathrm{u_2}\right) - r\,\mathrm{u_1}\right)^2\right)}{2} \\ &+ \frac{\mathrm{m_1}\,\left(\left(\mathrm{c_1}\,\sin(\mathrm{q_1} - \mathrm{q_2}) - \mathrm{w_1}\,\cos(\mathrm{q_1} - \mathrm{q_2})\right)^2\,\left(\mathrm{u_1} - \mathrm{u_2}\right)^2\right)}{2} + \frac{\mathrm{I_2}\,{\mathrm{u_1}}^2}{2} + \frac{\mathrm{I_1}\,\left(\mathrm{u_1} - \mathrm{u_2}\right)^2}{2} \\ &+ \frac{\mathrm{m_2}\,\left({\mathrm{u_1}}^2\,\left(\mathrm{c_2}\,\sin(\mathrm{q_1}) - \mathrm{w_2}\,\cos(\mathrm{q_1})\right)^2 + \left(r\,\mathrm{u_1} - \mathrm{u_1}\,\left(\mathrm{c_2}\,\cos(\mathrm{q_1}) + \mathrm{w_2}\,\sin(\mathrm{q_1})\right)\right)^2\right)}{2} \\ &- g\,\mathrm{m_1}\,\left(\cos(\gamma)\,\left(\mathrm{c_1}\,\cos(\mathrm{q_1} - \mathrm{q_2}) - r + \mathrm{w_1}\,\sin(\mathrm{q_1} - \mathrm{q_2})\right)\right. \\ &\qquad\qquad \left. - \sin(\gamma)\,\left(\mathrm{q_1}\,r - \mathrm{c_1}\,\sin(\mathrm{q_1} - \mathrm{q_2}) + \mathrm{w_1}\,\cos(\mathrm{q_1} - \mathrm{q_2})\right)\right) \\ &+ g\,\mathrm{m_2}\,\left(\sin(\gamma)\,\left(\mathrm{q_1}\,r - \mathrm{c_2}\,\sin(\mathrm{q_1}) + \mathrm{w_2}\,\cos(\mathrm{q_1})\right) - \cos(\gamma)\,\left(\mathrm{c_2}\,\cos(\mathrm{q_1}) - r + \mathrm{w_2}\,\sin(\mathrm{q_1})\right)\right) \end{aligned}$$

3.4 Front-leg Stop Transition (see Fig. 5 (f))

A mechanical stop restricts the angle between the legs to α. The front-leg stop transition occurs when the swing leg, body+front-leg, reaches the angle limit, i.e., $q_2 = -\alpha$. The stance leg angle remains unchanged between the transition, but the stance leg velocity undergoes a discrete change.

The stance leg velocity after transition is found using conservation of angular momentum about the pin joint H (see Fig. 6 (b)), $\overrightarrow{H}^{+}_{/H}=\overrightarrow{H}^{-}_{/H}$. The equations are

$$q_1^+ = q_1^-, \qquad Au_1^+ = b, \tag{4}$$
$$q_2^+ = -\alpha, \qquad u_2^+ = 0. \tag{5}$$

where A and b are given as follows

$$\begin{aligned} A = {} & I_1 + I_2 + \mathrm{m_2}\left(\left(\mathrm{c_2}\,\sin\left(\mathrm{q_1^+}\right) - \mathrm{w_2}\,\cos\left(\mathrm{q_1^+}\right)\right)^2 + \left(\mathrm{c_2}\,\cos\left(\mathrm{q_1^+}\right) - r + \mathrm{w_2}\,\sin\left(\mathrm{q_1^+}\right)\right)^2\right) \\ & + \mathrm{m_1}\left(\left(\mathrm{c_1}\,\cos\left(\mathrm{q_1^+} - \mathrm{q_2^+}\right) - r + \mathrm{w_1}\,\sin\left(\mathrm{q_1^+} - \mathrm{q_2^+}\right)\right)^2 + \left(\mathrm{c_1}\,\sin\left(\mathrm{q_1^+} - \mathrm{q_2^+}\right) - \mathrm{w_1}\,\cos\left(\mathrm{q_1^+} - \mathrm{q_2^+}\right)\right)^2\right) \end{aligned}$$

$$\begin{aligned} b = {} & \mathrm{m_1}\left(\left(\left(\mathrm{c_1}\,\cos\left(\mathrm{u_1^-} - \mathrm{q_2^-}\right) + \mathrm{w_1}\,\sin\left(\mathrm{q_1^-} - \mathrm{q_2^-}\right)\right)\left(\mathrm{u_1^-} - \mathrm{u_2^-}\right) - r\,\mathrm{u_1^-}\right)\left(\mathrm{c_1}\,\cos\left(\mathrm{q_1^-} - \mathrm{q_2^-}\right) - r\right. \right. \\ & \left. \left. + \mathrm{w_1}\,\sin\left(\mathrm{q_1^-} - \mathrm{q_2^-}\right)\right) + \left(\mathrm{c_1}\,\sin\left(\mathrm{q_1^-} - \mathrm{q_2^-}\right) - \mathrm{w_1}\,\cos\left(\mathrm{q_1^-} - \mathrm{q_2^-}\right)\right)^2\left(\mathrm{u_1^-} - \mathrm{u_2^-}\right)\right) \\ & + \mathrm{m_2}\left(\mathrm{u_1^-}\left(\mathrm{c_2}\,\cos\left(\mathrm{q_1^-}\right) - r + \mathrm{w_2}\,\sin\left(\mathrm{q_1^-}\right)\right)^2 + \mathrm{u_1^-}\left(\mathrm{c_2}\,\sin\left(\mathrm{q_1^-}\right) - \mathrm{w_2}\,\cos\left(\mathrm{q_1^-}\right)\right)^2\right) \\ & + I_2 u_1^- + I_1(u_1^- - u_2^-) \end{aligned}$$

3.5 One DOF, Rear Leg Stance (see Fig. 5 (g))

In this phase, the rear-leg is the stance leg (see Fig. 6 (b)) and the body+front-leg is held at fixed angle to the stance leg due to the mechanical stop. Thus, the dynamics of the system are due to q_1, whereas $q_2 = -\alpha$ and $u_2 = 0$. The equations are

$$A\ddot{q}_1 = b,$$
$$\ddot{q}_2 = 0.$$

The first equation used angular momentum balance about the contact point $\dot{\overrightarrow{H}}_{/P} = \overrightarrow{M}_{/P}$ and second equation is because the swing leg is stationary relative to the stance leg. The A and b matrices are

$$\begin{aligned} A = {} & -I_1 - I_2 + 2\,\mathrm{c_1}\,\mathrm{m_1}\,r\,\cos(\mathrm{q_1}) - \mathrm{c_2}^2\,\mathrm{m_2} - \mathrm{m_1}\,r^2 - \mathrm{m_2}\,r^2 - \mathrm{m_1}\,\mathrm{w_1}^2 - \mathrm{m_2}\,\mathrm{w_2}^2 \\ & - \mathrm{c_1}^2\,\mathrm{m_1} + 2\,\mathrm{m_1}\,r\,\mathrm{w_1}\,\sin(\mathrm{q_1}) + 2\,\mathrm{c_2}\,\mathrm{m_2}\,r\,\cos(\mathrm{q_1} - \mathrm{q_2}) + 2\,\mathrm{m_2}\,r\,\mathrm{w_2}\,\sin(\mathrm{q_1} - \mathrm{q_2}) \end{aligned}$$

$$\begin{aligned} b = {} & g\,\mathrm{m_1}\,r\,\sin(\gamma) - g\,\mathrm{m_2}\,\mathrm{w_2}\,\cos(\gamma - \mathrm{q_1} + \mathrm{q_2}) - \mathrm{c_2}\,g\,\mathrm{m_2}\,\sin(\gamma - \mathrm{q_1} + \mathrm{q_2}) \\ & + g\,\mathrm{m_2}\,r\,\sin(\gamma) - \mathrm{c_1}\,g\,\mathrm{m_1}\,\sin(\gamma - \mathrm{q_1}) - g\,\mathrm{m_1}\,\mathrm{w_1}\,\cos(\gamma - \mathrm{q_1}) + \mathrm{c_1}\,\mathrm{m_1}\,r\,\mathrm{u_1}^2\,\sin(\mathrm{q_1}) \\ & - \mathrm{m_1}\,r\,\mathrm{u_1}^2\,\mathrm{w_1}\,\cos(\mathrm{q_1}) + \mathrm{c_2}\,\mathrm{m_2}\,r\,\mathrm{u_1}^2\,\sin(\mathrm{q_1} - \mathrm{q_2}) - \mathrm{m_2}\,r\,\mathrm{u_1}^2\,\mathrm{w_2}\,\cos(\mathrm{q_1} - \mathrm{q_2}) \end{aligned}$$

The total energy at the beginning of this phase is found using the formula and using appropriate values for the state. Note that the formula is the same as $E_{b,c}$.

$$
\begin{aligned}
E = & \frac{\mathrm{I_1\,u_1}^2}{2} + \frac{\mathrm{I_2\,u_1}^2}{2} \\
& + \frac{\mathrm{m_1}\left(\mathrm{u_1}^2\left(\mathrm{c_1\,\sin(q_1 - q_2)} - \mathrm{w_1\,\cos(q_1 - q_2)}\right)^2 + \left(r\,\mathrm{u_1} - \mathrm{u_1}\,\left(\mathrm{c_1\,\cos(q_1 - q_2)} + \mathrm{w_1\,\sin(q_1 - q_2)}\right)\right)^2\right)}{2} \\
& + \frac{\mathrm{m_2}\left(\mathrm{u_1}^2\left(\mathrm{c_2\,\sin(q_1)} - \mathrm{w_2\,\cos(q_1)}\right)^2 + \left(r\,\mathrm{u_1} - \mathrm{u_1}\,\left(\mathrm{c_2\,\cos(q_1)} + \mathrm{w_2\,\sin(q_1)}\right)\right)^2\right)}{2} \\
& - g\,\mathrm{m_1}\,\left(\cos(\gamma)\,\left(\mathrm{c_1\,\cos(q_1 - q_2)} - r + \mathrm{w_1\,\sin(q_1 - q_2)}\right)\right. \\
& \qquad \left. - \sin(\gamma)\,\left(\mathrm{q_1}\,r - \mathrm{c_1\,\sin(q_1 - q_2)} + \mathrm{w_1\,\cos(q_1 - q_2)}\right)\right) \\
& + g\,\mathrm{m_2}\,\left(\sin(\gamma)\,\left(\mathrm{q_1}\,r - \mathrm{c_2\,\sin(q_1)} + \mathrm{w_2\,\cos(q_1)}\right) - \cos(\gamma)\,\left(\mathrm{c_2\,\cos(q_1)} - r + \mathrm{w_2\,\sin(q_1)}\right)\right)
\end{aligned}
$$

3.6 Rear-to-front Support Transition (see Fig. 5 (h))

We assume that the support transfer from rear-leg to body+front-leg occurs when the axis of the rear leg are vertical. Mathematically, the condition is given as follows, $q_1 - q_2 = \gamma$. The transition is smooth (i.e., there is no instantaneous change in angular velocity) because both legs have the same length and curvature. Because q_1 and q_2 denotes the position of the stance leg and swing leg respectively, we need to swap the roles of the legs. The conditions are

$$q_1^+ = q_1^- - q_2^-, \qquad u_1^+ = u_1^- - u_2^-, \tag{6}$$

$$q_2^+ = -q_2^- = \alpha, \qquad u_2^+ = -u_2^- = 0. \tag{7}$$

3.7 Two DOF, Front Leg Stance (see Fig. 5 (i))

In this phase, the body+front-leg is the stance leg (see Fig. 6 (a)) and the rear-leg is the swing leg. We obtain two equations by use angular momentum balance about the contact point, $\dot{\vec{H}}_{/P} = \vec{M}_{/P}$, and about the pin joint, $\dot{\vec{H}}_{/H} = \vec{M}_{/HP}$ (see Fig. 6 (a)). The equations are of the form

$$\mathbf{A}\ddot{\mathbf{q}} = \mathbf{b},$$

where $\mathbf{q} = \{q_1,\ q_2\}$, $\mathbf{A}$ is a 2x2 matrix, and $\mathbf{b}$ is a 2x1 vector. If $A_{i,j}$ is the element on the ith row and jth of $\mathbf{A}$, and if b_i is the ith row of $\mathbf{b}$ then

$$
\begin{aligned}
A_{1,1} = & -I_1 - I_2 + 2\,\mathrm{c_1\,m_1}\,r\,\cos(\mathrm{q_1}) - {\mathrm{c_2}}^2\,\mathrm{m_2} - \mathrm{m_1}\,r^2 - \mathrm{m_2}\,r^2 - \mathrm{m_1}\,{\mathrm{w_1}}^2 - \mathrm{m_2}\,{\mathrm{w_2}}^2 \\
& - {\mathrm{c_1}}^2\,\mathrm{m_1} + 2\,\mathrm{m_1}\,r\,\mathrm{w_1}\,\sin(\mathrm{q_1}) + 2\,\mathrm{c_2\,m_2}\,r\,\cos(\mathrm{q_1 - q_2}) + 2\,\mathrm{m_2}\,r\,\mathrm{w_2}\,\sin(\mathrm{q_1 - q_2})
\end{aligned}
$$

$$
\begin{aligned}
A_{1,2} &= -A_{2,1} \\
&= I_2 + \mathrm{m_2}\,\left({\mathrm{c_2}}^2 - r\,\cos(\mathrm{q_1 - q_2})\,\mathrm{c_2} + {\mathrm{w_2}}^2 - r\,\sin(\mathrm{q_1 - q_2})\,\mathrm{w_2}\right)
\end{aligned}
$$

$$A_{2,2} = I_2 + \mathrm{m_2}\,\left({\mathrm{c_2}}^2 + {\mathrm{w_2}}^2\right)$$

$$
\begin{aligned}
b_1 = -\mathrm{m}_2 \Big(& \left(\mathrm{c}_2 \sin(\mathrm{q}_1 - \mathrm{q}_2) - \mathrm{w}_2 \cos(\mathrm{q}_1 - \mathrm{q}_2)\right) \left(\mathrm{u}_1 - \mathrm{u}_2\right)^2 \left(\mathrm{c}_2 \cos(\mathrm{q}_1 - \mathrm{q}_2) - r + \mathrm{w}_2 \sin(\mathrm{q}_1 - \mathrm{q}_2)\right) \\
& - \left(\mathrm{c}_2 \cos(\mathrm{q}_1 - \mathrm{q}_2) + \mathrm{w}_2 \sin(\mathrm{q}_1 - \mathrm{q}_2)\right) \left(\mathrm{c}_2 \sin(\mathrm{q}_1 - \mathrm{q}_2) - \mathrm{w}_2 \cos(\mathrm{q}_1 - \mathrm{q}_2)\right) \left(\mathrm{u}_1 - \mathrm{u}_2\right)^2 \Big) \\
& - \mathrm{m}_1 \Big({\mathrm{u}_1}^2 \left(\mathrm{c}_1 \sin(\mathrm{q}_1) - \mathrm{w}_1 \cos(\mathrm{q}_1)\right) \left(\mathrm{c}_1 \cos(\mathrm{q}_1) - r + \mathrm{w}_1 \sin(\mathrm{q}_1)\right) \\
& \qquad - {\mathrm{u}_1}^2 \left(\mathrm{c}_1 \cos(\mathrm{q}_1) + \mathrm{w}_1 \sin(\mathrm{q}_1)\right) \left(\mathrm{c}_1 \sin(\mathrm{q}_1) - \mathrm{w}_1 \cos(\mathrm{q}_1)\right) \Big) \\
& - g\, \mathrm{m}_1 \left(\sin(\gamma) \left(\mathrm{c}_1 \cos(\mathrm{q}_1) - r + \mathrm{w}_1 \sin(\mathrm{q}_1)\right) - \cos(\gamma) \left(\mathrm{c}_1 \sin(\mathrm{q}_1) - \mathrm{w}_1 \cos(\mathrm{q}_1)\right)\right) \\
& - g\, \mathrm{m}_2 \left(\sin(\gamma) \left(\mathrm{c}_2 \cos(\mathrm{q}_1 - \mathrm{q}_2) - r + \mathrm{w}_2 \sin(\mathrm{q}_1 - \mathrm{q}_2)\right) - \cos(\gamma) \left(\mathrm{c}_2 \sin(\mathrm{q}_1 - \mathrm{q}_2) - \mathrm{w}_2 \cos(\mathrm{q}_1 - \mathrm{q}_2)\right)\right)
\end{aligned}
$$

$$
b_2 = g\, \mathrm{m}_2 \left(\cos(\gamma) \left(\mathrm{c}_2 \sin(\mathrm{q}_1 - \mathrm{q}_2) - \mathrm{w}_2 \cos(\mathrm{q}_1 - \mathrm{q}_2)\right) - \sin(\gamma) \left(\mathrm{c}_2 \cos(\mathrm{q}_1 - \mathrm{q}_2) + \mathrm{w}_2 \sin(\mathrm{q}_1 - \mathrm{q}_2)\right)\right)
$$

The total energy at the beginning of this phase is found using the formula and using appropriate values for the state.

$$
\begin{aligned}
E = & \frac{\mathrm{m}_2 \left(\left(\left(\mathrm{c}_2 \cos(\mathrm{q}_1 - \mathrm{q}_2) + \mathrm{w}_2 \sin(\mathrm{q}_1 - \mathrm{q}_2)\right) \left(\mathrm{u}_1 - \mathrm{u}_2\right) - r\, \mathrm{u}_1\right)^2\right)}{2} \\
& + \frac{\mathrm{m}_2 \left(\left(\mathrm{c}_2 \sin(\mathrm{q}_1 - \mathrm{q}_2) - \mathrm{w}_2 \cos(\mathrm{q}_1 - \mathrm{q}_2)\right)^2 \left(\mathrm{u}_1 - \mathrm{u}_2\right)^2\right)}{2} + \frac{\mathrm{I}_1 {\mathrm{u}_1}^2}{2} + \frac{\mathrm{I}_2 \left(\mathrm{u}_1 - \mathrm{u}_2\right)^2}{2} \\
& + \frac{\mathrm{m}_1 \left({\mathrm{u}_1}^2 \left(\mathrm{c}_1 \sin(\mathrm{q}_1) - \mathrm{w}_1 \cos(\mathrm{q}_1)\right)^2 + \left(r\, \mathrm{u}_1 - \mathrm{u}_1 \left(\mathrm{c}_1 \cos(\mathrm{q}_1) + \mathrm{w}_1 \sin(\mathrm{q}_1)\right)\right)^2\right)}{2} \\
& - g\, \mathrm{m}_2 \left(\cos(\gamma) \left(\mathrm{c}_2 \cos(\mathrm{q}_1 - \mathrm{q}_2) - r + \mathrm{w}_2 \sin(\mathrm{q}_1 - \mathrm{q}_2)\right) \right. \\
& \qquad \left. - \sin(\gamma) \left(\mathrm{q}_1\, r - \mathrm{c}_2 \sin(\mathrm{q}_1 - \mathrm{q}_2) + \mathrm{w}_2 \cos(\mathrm{q}_1 - \mathrm{q}_2)\right)\right) \\
& + g\, \mathrm{m}_1 \left(\sin(\gamma) \left(\mathrm{q}_1\, r - \mathrm{c}_1 \sin(\mathrm{q}_1) + \mathrm{w}_1 \cos(\mathrm{q}_1)\right) - \cos(\gamma) \left(\mathrm{c}_1 \cos(\mathrm{q}_1) - r + \mathrm{w}_1 \sin(\mathrm{q}_1)\right)\right)
\end{aligned}
$$

3.8 Rear-leg Stop Transition (see Fig. 5 (j))

The rear-leg stop transition occurs when the swing leg, rear-leg collides with the stance leg, the condition is $q_2 = 0$. The stance leg angle remains unchanged between the transition, but the stance leg velocity undergoes a discrete change. The stance leg velocity after transition is found using conservation of angular momentum about the pin joint H (see Fig. 6 (a)), $\overrightarrow{H}^{+}_{/H} = \overrightarrow{H}^{-}_{/H}$. The equations are

$$
q_1^+ = q_1^-, \qquad A u_1^+ = b, \tag{8}
$$

$$
q_2^+ = 0, \qquad u_2^+ = 0. \tag{9}
$$

where A and b are given as follows

$$
\begin{aligned}
A = & I_1 + I_2 + \mathrm{m}_1 \left(\left(\mathrm{c}_1 \sin\left(\mathrm{q}_1^+\right) - \mathrm{w}_1 \cos\left(\mathrm{q}_1^+\right)\right)^2 + \left(\mathrm{c}_1 \cos\left(\mathrm{q}_1^+\right) - r + \mathrm{w}_1 \sin\left(\mathrm{q}_1^+\right)\right)^2\right) \\
& + \mathrm{m}_2 \left(\left(\mathrm{c}_2 \cos\left(\mathrm{q}_1^+ - \mathrm{q}_2^+\right) - r + \mathrm{w}_2 \sin\left(\mathrm{q}_1^+ - \mathrm{q}_2^+\right)\right)^2 + \left(\mathrm{c}_2 \sin\left(\mathrm{q}_1^+ - \mathrm{q}_2^+\right) - \mathrm{w}_2 \cos\left(\mathrm{q}_1^+ - \mathrm{q}_2^+\right)\right)^2\right)
\end{aligned}
$$

$$
\begin{aligned}
b = & \mathrm{m}_2 \left(\left(\left(\mathrm{c}_2 \cos\left(\mathrm{q}_1^- - \mathrm{q}_2^-\right) + \mathrm{w}_2 \sin\left(\mathrm{q}_1^- - \mathrm{q}_2^-\right)\right) \left(\mathrm{u}_1^- - \mathrm{u}_2^-\right) - r\, \mathrm{u}_1^-\right) \left(\mathrm{c}_2 \cos\left(\mathrm{q}_1^- - \mathrm{q}_2^-\right) - r \right. \right. \\
& \left. \left. + \mathrm{w}_2 \sin\left(\mathrm{q}_1^- - \mathrm{q}_2^-\right)\right) + \left(\mathrm{c}_2 \sin\left(\mathrm{q}_1^- - \mathrm{q}_2^-\right) - \mathrm{w}_2 \cos\left(\mathrm{q}_1^- - \mathrm{q}_2^-\right)\right)^2 \left(\mathrm{u}_1^- - \mathrm{u}_2^-\right)\right) \\
& + \mathrm{m}_1 \left(\mathrm{u}_1^- \left(\mathrm{c}_1 \cos\left(\mathrm{q}_1^-\right) - r + \mathrm{w}_1 \sin\left(\mathrm{q}_1^-\right)\right)^2 + \mathrm{u}_1^- \left(\mathrm{c}_1 \sin\left(\mathrm{q}_1^-\right) - \mathrm{w}_1 \cos\left(\mathrm{q}_1^-\right)\right)^2\right) \\
& + I_1 u_1^- + I_2 (u_1^- - u_2^-)
\end{aligned}
$$

References

[1] Pranav Bhounsule. Matlab simulation of a passive dynamic walker. https://github.com/pab47/RowdyWalker, Accessed March 2018.

[2] UTSA. Roadrunner graphic. http://www.utsa.edu/ucm/resources/identity/visual-style/roadrunner.html, Accessed February 2016 2016.